Follow-up of a panel restoration procedure through image correlation and finite element modeling

David Dureisseix, Julien Colmars, Adrien Baldit, Fabrice Morestin, Hubert Maigre

Follow-up of a panel restoration procedure through image correlation and finite element modeling

D. Dureisseix[*], J. Colmars[†], A. Baldit[†], F. Morestin[*], H. Maigre[*]

January 28, 2011

Abstract

Residual stress estimation is an important question for structural integrity. Since residual stresses are self-balanced stress fields, a classical way to obtain information on them is to remove a part of the structure, and observe the structure displacement field arising from the stress redistribution. The hole-drilling method is such an approach. In some cases, as for the present one concerning a painted panel of cultural heritage, the hole-drilling method is not suited (a structure with a complex geometry, few tests allowed) but one can take advantage of structural modifications if they are monitored (here, a restoration act). We therefore describe in this article a model updating approach, focusing on the residual stress estimation and not on the material parameter identification.

This study couples an optical non-invasive shape measurement (digital image correlation, using a projected speckle pattern on the painted panel, with luminance compensation) and a numerical approach (3D finite elements) for the model updating. The 3D stereo-correlation is used to measure a partial displacement field between three different states of the structure (at three different times of the restoration act). The numerical part concerns stress evaluation, once the model and the experiments are compared using a geometric mapping and a spatial projection of discrete fields. Using modeling and identification, the simulation is used to obtain the residual stresses in the panel, before and after the restoration.

This article in its final form was published in *International Journal of Solids and Structures*, Volume 48, 2011, Pages 1024-1033.
http://www.elsevier.com
doi:10.1016/j.ijsolstr.2010.12.010
pii:S0020-7683(10)00446-4

keyword residual stresses, wood panel, painting, conservation, cultural heritage, stereocorrelation, identification, inverse problem

MSC 2010 65N21, 74B10, 74S05, 74G75, 65D18

[*]Laboratoire de Mécanique des Contacts et des Structures (LaMCoS), INSA Lyon / CNRS UMR 5259, 18-20 rue des Sciences, F-69621 VILLEURBANNE CEDEX, FRANCE

[†]Laboratoire de Mécanique et Génie Civil (LMGC), Montpellier 2 University / CNRS UMR 5508, CC 048, place Eugène Bataillon, F-34095 MONTPELLIER CEDEX 5, FRANCE

Figure 1: *Baptême du Christ*, Palais du Roure, Avignon, France (left) and its cradle (right)

1 Introduction

Conservation of paintings of cultural heritage on wood panels could gain from using tools of wood science and structural mechanics, to guide decision for curators and restorers. Indeed, the consequences of a restoration act on the future integrity of an artwork can be assessed with virtual (numerical) simulation once a predictive model has been designed. Such numerical simulations in the same context have recently been used for painted panels, for instance in [10, 8, 16], for musical instruments, [22, 14], for other wooden structures, [3, 7], for ancient buildings, [17, 20, 28], and even for natural parks [6].

Since each artwork is a particular case, it requires an identification step to nurture the model. Objects of cultural heritage are often unique and precious artworks, and few mechanical tests can be conducted to identify the present state of the structure, that cannot be estimated with the evolution it was subjected to, due to the lack of past measurements. The present study mainly deals with a model design, based on finite elements, to couple simulations and experiments during a particular restoration act. The concerned artwork is 'Baptême du Christ', from an anonymous artist, stored in 'Palais du Roure', Avignon, France, Figure 1-left.

An early restoration act, performed in the 70s but typical of the 19th and beginning of the 20th century, was a french parquetage (or cradle) on the rear side of the painted panel. This cradle consists of eight vertical beech beams, glued on the panel rear side (485 mm $\times$ 405 mm $\times$ 12 mm), and crossed with eight horizontal beech beams, Figure 1-right. This kind of restoration aims to rigidify the wooden support to avoid excessive movements (mainly bending due to dissymmetry in moisture exchanges on both sides of the panel) that may endangers the pictural layer. The drawback of such a rigidification is the increase in internal stresses with humidity variations of the environment, see [21]. Moreover this panel exhibits two cracks; they will not be taken into account herein.

The new restoration act dates back to 2007 and has been followed in this

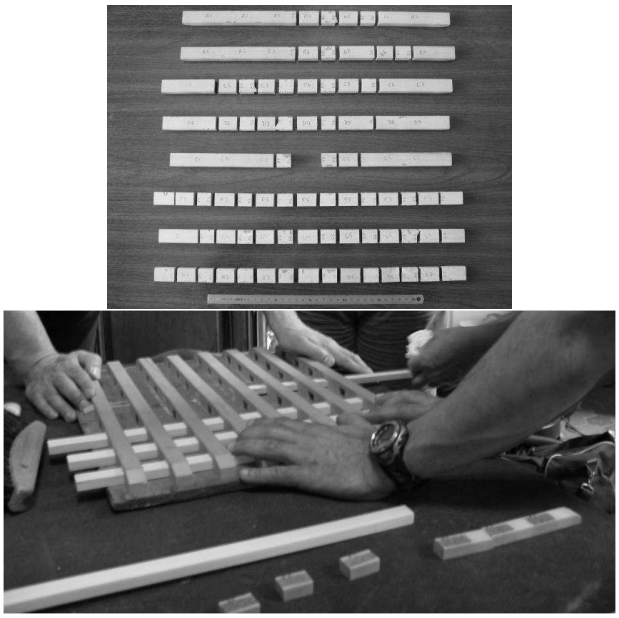

Figure 2: Former horizontal beams (left), cut to be extracted (central part missing, used for material identification) and replacement of horizontal beams

study: the replacement of the horizontal beams of the cradle by new ones made in spruce. The initial horizontal beams were partly glued and partly clamped due to a permanent long-term deformation of the panel that installed itself after the initial restoration (mainly due to the mechanosorption effect). For the former beams to be replaced, they had to be cut, Figure 2. This illustrates the presence of internal (or residual) stresses. The restoration has been monitored with image analysis: the shape of a part of the front painted side has been measured (i) before the removing of the former horizontal beams, (ii) after this removing and (iii) after mounting the new horizontal beams. These experimental data has to be used in conjunction with a structural analysis, in order to estimate the residual stresses in the panel, which is one of the goals of this study. Section 2 describes the experimental technique, while Section 3 focuses on the finite element model and its comparison to the measurements. Finally, Section 4 uses these tools for the residual stresses estimation.

2 Shape measurement with 3D stereo-correlation

This non-invasive optical technique allows measuring a 3D shape of a part of the surface of a structure. For artworks of cultural heritage, this technique is useful since no contact with the artwork is needed; nevertheless, no continuous measures can be obtained along time, only several ones at particular instants, due to the delay needed to install and calibrate the acquisition chain which is composed (Figure 3) at least of:

- two stereoscopic cameras,

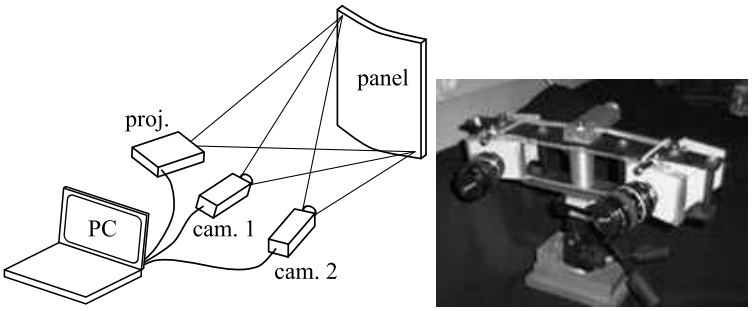

Figure 3: Principles of the measurement technique (left) and stereo cameras (right)

- a video beam projector,
- a processing unit (computer) to capture and correlate images from the cameras.

With two camera images taken from different points of view, the 3D position of visible and identifiable points (or patches) can be obtained by image correlation. The basic images of the artwork cannot be used due to too much contrast on the pictural layer, between large surfaces of too small contrast (aplats or flat tints). Therefore, a more suited pattern (classically a speckle pattern) should be substituted to the original image of the panel. Since no physical speckle pattern can be marked on the painting, a virtual speckle pattern image is projected onto the painted surface, once the initial painting is virtually rubbed out. To do so, an initial image is taken, is numerically treated to produce a 'negative' image that is back-projected to the panel to compensate the initial picture luminance (this is the so-called 'extinction' of the painting). The virtual speckle pattern is then added to the projection to appear on the panel, Figure 4. The correlation of the images taken from this virtual speckle pattern by the two cameras allows to derive the 3D position of patches of pixels, as in [15]. This leads to approx. 80 000 3D point locations on a large part of the pictural layer (not up to the border, nevertheless).

Three different measures have been taken:

- one before the restoration act; this artwork state will then be denoted with $\Omega^{(1)}$;
- one with the horizontal beams removed, which panel state denoted with $\Omega^{(2)}$; and
- one with the new horizontal beams mounted, denoted with $\Omega^{(3)}$.

Apart from an image distortion correction (with the help of a calibration before any data capture), the position of the centers of pixel patches (which are the measured points) are finally converted into physical length in the coordinate system related to one of the cameras. Since, for each of the measured states, the panel may be not repositioned at the same location, each measure is assumed to posses its own coordinate system.

Figure 4: Left camera, after beam removal: initial image capture (left) and projected speckle pattern on the luminance-compensated image (right)

3 Finite element model and model updating

3.1 Ideal geometry and wood behavior

For practical reasons, a finite element model has been design on an ideal geometry (i.e. a perfectly flat and rectangular panel), Figure 5. This particular state of the artwork, though not physically interesting, will be the reference state for computations, and will be denoted with $\Omega^{(0)}$.

More precisely, the notation $\Omega^{(j)}$ will denote the state (j) on the structure composed of the panel and the vertical beams, while the set of horizontal beams will be denoted with $\Omega'^{(j)}$ when needed. These two structures can be seen as two subdomains, and the interface between them will be denoted with Γ, Figure 5.

Assuming that all the previously mentioned states $\Omega^{(j)}$ are not too far from the reference state $\Omega^{(0)}$, the small displacement and small strain assumptions hold, and all the finite element displacement fields will be defined on this reference state, as for the material characteristic coefficients. In this study, we expect the restoration act to be sufficiently short to neglect the relative humidity changes of the environment which the wood is sensitive to. Since only elasticity is modeled herein, other mechanical behavior such as viscoelasticity is neglected for sake of simplicity, though its characteristic time may be of the same order of magnitude that the restoration duration. Nevertheless, this assumption is conservative, since the residual stresses tend to relax in presence of viscoelasticity.

For the panel, once the sawn on the initial trunk is known, the elastic characteristics are selected as for a standard coniferous wood: spruce from [11], Table 1. The elastic behavior is orthotropic, and heterogeneous (the local anisotropic basis changes with the considered point). The position of the tree center is determined with observation of the growth rings on the RT (radial-tangential) section: an off-plane of 125 mm is obtained, Figure 6.

The beams are assumed to be homogeneous, sawn along the L (longitudinal) direction. Displacement fields with respect to the reference state are denoted

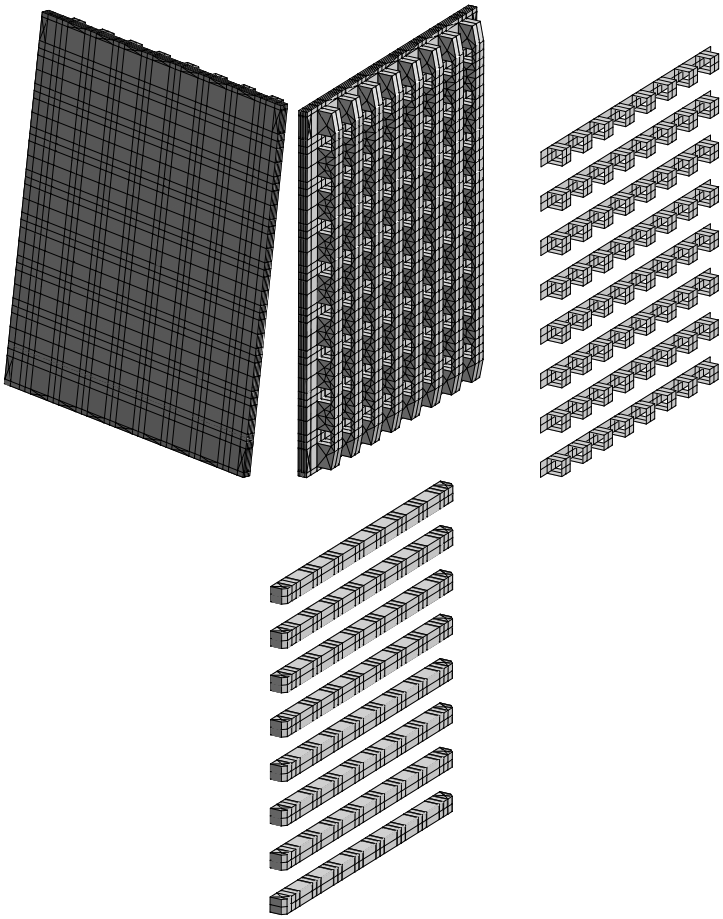

Figure 5: Finite element model of the ideal geometry for the panel and vertical beams $\Omega^{(0)}$ (left two images), interface Γ (center), horizontal beams (right) $\Omega'^{(0)}$

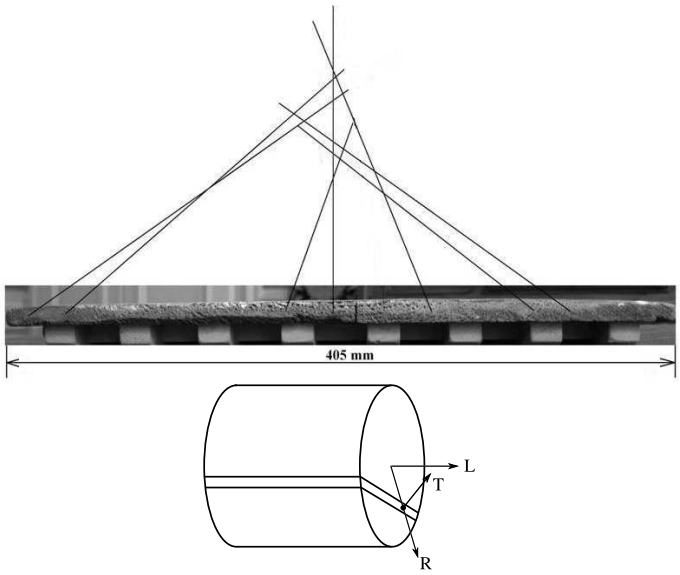

Figure 6: Determination of local anisotropic basis with growth ring observation

with $\underline{\bar{U}}^{(j)}$. Since state $\Omega^{(2)}$ will play a particular role in the following, the displacements with respect to $\Omega^{(2)}$ are also of interest: they are denoted with $\underline{U}^{(j)}$; indeed: $\underline{U}^{(j)} = \underline{\bar{U}}^{(j)} - \underline{\bar{U}}^{(2)}$.

3.2 Matching experimental points and finite element nodes

Each measured set of points is related to its own coordinate system, which are in turn different from the coordinate system used for the ideal geometry $\Omega^{(0)}$. Therefore each measured set (j) has to be matched to the state $\Omega^{(0)}$ in order to define the partial finite element field of measured values $\underline{\bar{U}}_m^{(j)}$. Note that these measurements are partial information since the displacement is measured only

species	spruce	beech
H / %	13.1	9.4
ρ / g/cm^3	0.31	0.63
E_R / MPa	816	2 040
E_T / MPa	304	867
E_L / MPa	8 020	14 100
G_{RT} / MPa	48	500
G_{TL} / MPa	461	980
G_{RL} / MPa	558	1 850
ν_{RT}	0.67	0.73
ν_{LT}	0.33	0.46
ν_{LR}	0.34	0.36

Table 1: Material elastic parameters after [11] (for standard relative humidity H and specific density ρ)

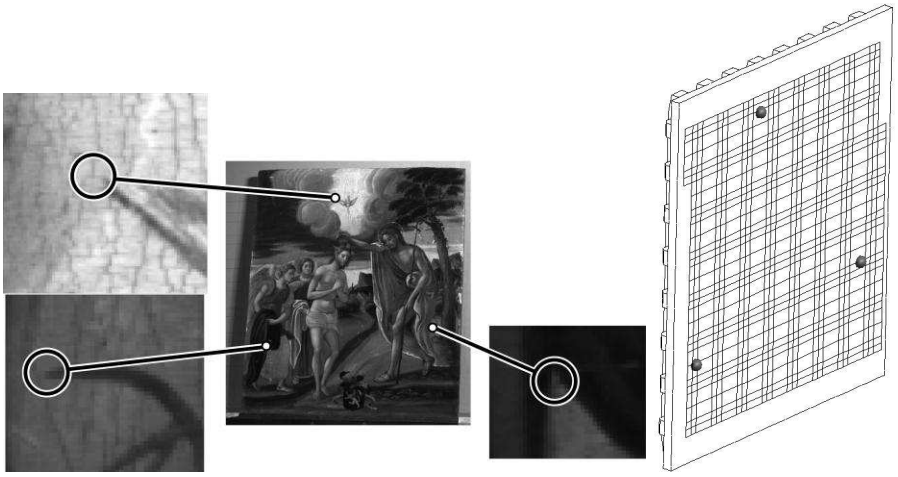

Figure 7: Reference points (left) and measured field projected onto the finite element mesh (right) for the initial state, with its own reference points

of a part of the boundary, and that only the out-of-plane component of the displacements are obtained, because the speckle pattern is not bonded onto the panel, but merely projected on it.

To get these partial finite element fields of measured values, three reference points are selected in order to be easily located on pixelized images, both on the states $\Omega^{(j)}$ with coordinates $X^{(j)}$ and on a frontal image identified as $\Omega^{(0)}$ with coordinates $X^{(0)}$, Figure 7.

The transformation mapping $X^{(j)}$ to $X^{(0)}$ is expected to be composed of a translation $T^{(j)}$ and a finite rotation $\boldsymbol{R}^{(j)}$. The translation links the centroids of the set of reference points. The finite rotation may be defined for instance with a polar decomposition of the mapping; in this case, we consider that the three reference points define a plane into which each point $M^{(j)}$ has barycentric coordinates λ: $M^{(j)} = \boldsymbol{X}^{(j)}\lambda$. With independent points, $\lambda = \boldsymbol{A}^{-1}{\boldsymbol{X}^{(j)}}^T M^{(j)}$ with $\boldsymbol{A} = {\boldsymbol{X}^{(j)}}^T\boldsymbol{X}^{(j)}$. The transformation is expected to map $M^{(j)}$ to $M^{(0)} = \boldsymbol{X}^{(0)}\lambda = \boldsymbol{F}^{(j)}M^{(j)}$ with the gradient of the transformation: $\boldsymbol{F}^{(j)} = \boldsymbol{X}^{(0)}\boldsymbol{A}^{-1}{\boldsymbol{X}^{(j)}}^T$. A polar decomposition of $\boldsymbol{F}^{(j)}$ produces the rotation $\boldsymbol{R}^j$. Unfortunately, this rotation may be composed with a planar symmetry, which is cumbersome to eliminate, see [19, 25]. We therefore preferred a simple Gram-Schmidt orthogonalization $\boldsymbol{E}^{(j)}$ of the basis generated by $\boldsymbol{X}^{(j)}$ (and $\boldsymbol{E}^{(0)}$ accordingly). In such a case, the previous approach leads to: $\boldsymbol{F}^{(j)} = \boldsymbol{E}^{(0)}{\boldsymbol{E}^{(j)}}^{-1}$ which is exactly the rotation $\boldsymbol{R}^{(j)}$.

Then, the coordinates of all measured points can be transformed to lie in the coordinate system of $\Omega^{(0)}$. Finally, the normal coordinate to the plane of the panel is interpolated at each possible finite element node of the painted side to get a field of normal displacement $\underline{z}^T\underline{\bar{U}}_m^{(j)}$, Figure 8, where $\underline{z}^T$ denotes the normal to the panel.

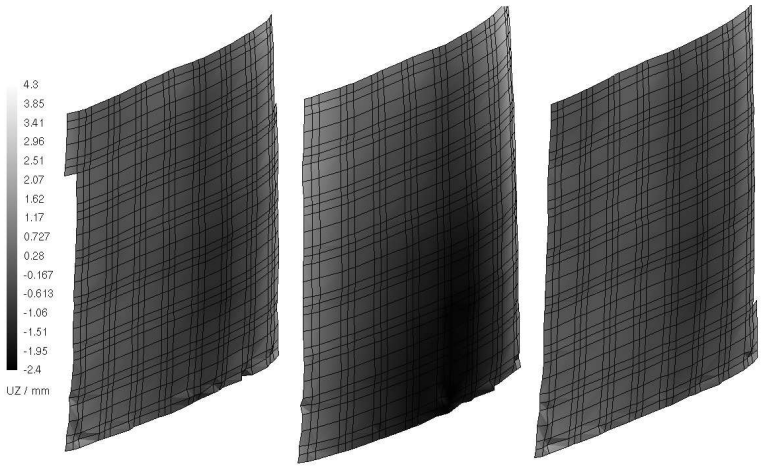

Figure 8: Measured fields projected onto the finite element mesh: initial state (left), after beam removal (middle), and after beam replacement (right). Displacement amplified 8 times.

3.3 Model updating

Once the partial shape of the different states $\Omega^{(j)}$ of the structure composed by the panel and the vertical beams, $\underline{z}^T\underline{\bar{U}}_m^{(j)}$ or $\underline{z}^T\underline{U}_m^{(j)} = \underline{z}^T\underline{\bar{U}}_m^{(j)} - \underline{z}^T\underline{\bar{U}}_m^{(2)}$, have been obtained, these different states have to be reconstructed from the ideal geometry: this is the model updating stage. Since the small displacement assumption holds, the shape updating reduces to find a finite element displacement on the undistorted ideal geometry: $\underline{\bar{U}}^{(j)}(M)$, $M \in \Omega^{(0)}$. The column vector of the corresponding nodal displacements is denoted with $\bar{\boldsymbol{u}}^{(j)}$. These degrees of freedom (dof) can be split in several sets. First, the dofs at the interface between the panel (with vertical beams) and the horizontal beams are denoted with a subscript Γ. The remaining dofs are denoted with a subscript i; they are themselves split into measured dofs with a subscript c (these dofs are only the out-of-plane component of the displacement at measured nodes), and the non-measured dofs with a subscript r. The measured partial shapes at finite element nodes are stored in column vectors $\bar{\boldsymbol{u}}_m^{(j)}$ or $\boldsymbol{u}_m^{(j)}$. Finally, we can define $\boldsymbol{C}^{(j)}$ as the Boolean mapping matrix on c dofs (measured dofs), such that $\bar{\boldsymbol{u}}_c^{(j)} = \boldsymbol{C}^{(j)}\bar{\boldsymbol{u}}^j$. The superscript (j) is omitted in the following.

For each state Ω, a part of its boundary is the interface with the horizontal beams Γ; the remaining part, $\partial_2\Omega$, is supposed to be traction-free. We will neglect the body forces due to gravity in the following; indeed, all the measurements are performed on the panel in up-right position, therefore the vertical compressive stress on a cross-section S is bounded with $\sigma = mg/S$; with a mass of the artwork $m \approx 3$ kg, one gets $\sigma \approx 6$ kPa which will be negligible with respect to the residual stress to be estimated. On the interface Γ, the structure is submitted to the action of the set of horizontal beams; these may consist of a displacement $\underline{U}_\Gamma$ and a force density $\underline{F}_\Gamma$ defined on this interface. The techniques that will be used in the following are derived from model identification techniques as in [4, 12, 1]. A couple of displacements $(\underline{U}, \underline{U}_\Gamma)$ will be said

kinematically admissible (KA) simply if $\underline{U} = \underline{U}_\Gamma$ on Γ. A couple of stress and interface forces $(\boldsymbol{\sigma}, \underline{F}_\Gamma)$ will be said statically admissible (SA) if: $\underline{\mathrm{div}}\,\boldsymbol{\sigma} = 0$ in Ω, $\boldsymbol{\sigma}\underline{n} = 0$ on $\partial_2\Omega$, and $\boldsymbol{\sigma}\underline{n} = \underline{F}_\Gamma$ on Γ. $\underline{n}$ is the unitary normal vector to the boundary, pointing out of Ω.

A mechanical state of the studied structure consists of two couples, $(\underline{U}, \underline{U}_\Gamma)$ KA and $(\boldsymbol{\sigma}, \underline{F}_\Gamma)$ SA, satisfying the constitutive relation, here the elastic behavior: $\boldsymbol{\sigma} = \boldsymbol{D}\boldsymbol{\varepsilon}(\underline{U})$ in Ω. In other words, the following constitutive relation error should be null:

$$\int_\Omega e^2(\boldsymbol{\sigma}, \underline{U}) d\Omega = 0 \tag{1}$$

with

$$e^2(\boldsymbol{\sigma}, \underline{U}) = \frac{1}{2}[\boldsymbol{\sigma} - \boldsymbol{D}\boldsymbol{\varepsilon}(\underline{U})] : \boldsymbol{D}^{-1}[\boldsymbol{\sigma} - \boldsymbol{D}\boldsymbol{\varepsilon}(\underline{U})] \tag{2}$$

When dealing with model updating, the mechanical state has moreover to cope with the measured quantities, here: the measured displacement field $\underline{z}^T\underline{U}_m$ on $\partial_m\Omega$. Both the model and the measured cannot be perfect, therefore one seeks for a compromise between all the constraints to be satisfied. The model updating proposed approach consists in balancing the verification of the constitutive relation and the measures, by searching the couples $(\underline{U}, \underline{U}_\Gamma)$ and $(\boldsymbol{\sigma}, \underline{F}_\Gamma)$ as:

$$\underset{\substack{(\underline{U}, \underline{U}_\Gamma) \text{ KA} \\ (\boldsymbol{\sigma}, \underline{F}_\Gamma) \text{ SA}}}{\operatorname{argmin}} \int_\Omega e^2(\boldsymbol{\sigma}, \underline{U}) d\Omega + \alpha \int_{\partial_m\Omega} e_m^2(\underline{U}) dS \tag{3}$$

in which the term e_m is an error with respect to the measures, for instance:

$$e_m^2(\underline{U}) = \frac{1}{2}[\underline{z}^T(\underline{U} - \underline{U}_m)]\omega[\underline{z}^T(\underline{U} - \underline{U}_m)] \tag{4}$$

ω is a scalar field of weighting terms, taking its values in $[0, 1]$, to take into account confidence levels in the experimental values. α is a singe scalar coefficient (homogeneous to a stiffness) to balance the two terms in the functional, or the cost function, to be minimized (3). These parameters will be precised in the following.

Note that this problem is not in a closed form until additional informations are stated on the interface fields $(\underline{U}_\Gamma, \underline{F}_\Gamma)$.

Dealing with finite element numerical approximations is easy for the kinematically admissible couples: the displacements $(\underline{U}, \underline{U}_\Gamma)$ are replaced by their finite element approximations counterparts $(\boldsymbol{u}, \boldsymbol{u}_\Gamma)$. For the stress field, an additional approximation is to assume a special form, deriving from a displacement field $\underline{V}$: $\boldsymbol{\sigma} = \boldsymbol{D}\boldsymbol{\varepsilon}(\underline{V})$, which is in turn classically discretized by finite elements into $\boldsymbol{v}$. $\boldsymbol{D}(M)$ is the Hooke operator field on the panel and the vertical beams, modeling the elastic behavior of the wood material.

The static admissibility is therefore replaced with its finite element approximation: denoting with $\boldsymbol{f}_\Gamma$ the generalized nodal forces associated to $\underline{F}_\Gamma$, $(\boldsymbol{v}, \boldsymbol{f}_\Gamma)$ will be said statically admissible (SA), if:

$$\boldsymbol{K}\boldsymbol{v} = \begin{bmatrix} \boldsymbol{K}_{ii} & \boldsymbol{K}_{i\Gamma} \\ \boldsymbol{K}_{\Gamma i} & \boldsymbol{K}_{\Gamma\Gamma} \end{bmatrix} \begin{bmatrix} \boldsymbol{v}_i \\ \boldsymbol{v}_\Gamma \end{bmatrix} = \begin{bmatrix} \boldsymbol{0} \\ \boldsymbol{f}_\Gamma \end{bmatrix}$$

or

$$\boldsymbol{K}\boldsymbol{v} = \begin{bmatrix} \boldsymbol{K}_{rr} & \boldsymbol{K}_{rc} & \boldsymbol{K}_{r\Gamma} \\ \boldsymbol{K}_{cr} & \boldsymbol{K}_{cc} & \boldsymbol{K}_{c\Gamma} \\ \boldsymbol{K}_{\Gamma r} & \boldsymbol{K}_{\Gamma c} & \boldsymbol{K}_{\Gamma\Gamma} \end{bmatrix} \begin{bmatrix} \boldsymbol{v}_r \\ \boldsymbol{v}_c \\ \boldsymbol{v}_\Gamma \end{bmatrix} = \begin{bmatrix} \boldsymbol{0} \\ \boldsymbol{0} \\ \boldsymbol{f}_\Gamma \end{bmatrix} \tag{5}$$

where $\boldsymbol{K}$ is the finite element stiffness matrix, arising from Hooke operator $\boldsymbol{D}$. Note that this implies:

$$\boldsymbol{v} = \begin{bmatrix} \boldsymbol{v}_i \\ \boldsymbol{v}_\Gamma \end{bmatrix} = \boldsymbol{A}_\Gamma \boldsymbol{v}_\Gamma \quad \text{with} \quad \boldsymbol{A}_\Gamma = \begin{bmatrix} -\boldsymbol{K}_{ii}^{-1}\boldsymbol{K}_{i\Gamma} \\ \boldsymbol{1} \end{bmatrix} \tag{6}$$

$\boldsymbol{A}_\Gamma^T \boldsymbol{K} \boldsymbol{A}_\Gamma = \boldsymbol{K}_{\Gamma\Gamma}^\star$ (where a superscript T denotes the transposition) is the so-called Schur complement of $\boldsymbol{K}$ on Γ dofs, and finally the discretized static admissibility is merely a relationship between displacements and forces at the interface: $\boldsymbol{K}_{\Gamma\Gamma}^\star \boldsymbol{v}_\Gamma = \boldsymbol{f}_\Gamma$.

The model updating now consists in finding:

$$\begin{array}{c} \underset{\boldsymbol{u}}{\text{argmin}} \quad f(\boldsymbol{u}, \boldsymbol{v}) \\ (\boldsymbol{v}, \boldsymbol{f}_\Gamma) \text{ SA} \end{array} \tag{7}$$

with

$$f(\boldsymbol{u}, \boldsymbol{v}) = \frac{1}{2}(\boldsymbol{u} - \boldsymbol{v})^T \boldsymbol{K} (\boldsymbol{u} - \boldsymbol{v}) + \frac{1}{2}\alpha (\boldsymbol{C}\boldsymbol{u} - \boldsymbol{u}_m)^T \boldsymbol{\omega} (\boldsymbol{C}\boldsymbol{u} - \boldsymbol{u}_m) \tag{8}$$

$\boldsymbol{u}$ is a kinematically admissible (KA) field, expected to be close to the measurements $\boldsymbol{u}_m$. This is a balance between a smooth field (according to equilibrium equations, thanks to the first term), and a field matching measurements (according to the second term). $\boldsymbol{\omega}$ is a diagonal weighting matrix (with entries ω in [0,1]). We may interpret either the field $\boldsymbol{u}$ or $\boldsymbol{v}$ as a smoothing and a prolongation of $\boldsymbol{u}_m$ on the whole structure.

The coefficient α can be estimated by using a collocated prolongation of the measurement: $\hat{\boldsymbol{u}} = \boldsymbol{A}_c \boldsymbol{u}_m$, where $\boldsymbol{A}_c$ is defined similarly as $\boldsymbol{A}_\Gamma$, but with the set of measured dofs on Ω replacing Γ:

$$\alpha = \frac{\hat{\boldsymbol{u}}^T \boldsymbol{K} \hat{\boldsymbol{u}}}{\boldsymbol{u}_m^T \boldsymbol{K} \boldsymbol{u}_m} = \frac{\boldsymbol{u}_m^T \boldsymbol{A}_c^T \boldsymbol{K} \boldsymbol{A}_c \boldsymbol{u}_m}{\boldsymbol{u}_m^T \boldsymbol{K} \boldsymbol{u}_m} = \frac{\boldsymbol{u}_m^T \boldsymbol{K}_{cc}^\star \boldsymbol{u}_m}{\boldsymbol{u}_m^T \boldsymbol{K} \boldsymbol{u}_m} \tag{9}$$

Eventually, it can be adjusted by iterating the identification procedure a few times.

The choice of the diagonal weighting $\boldsymbol{\omega}$ is part of the modeling. It may take into account the reliability in the measurements (a value 1 is a maximal confidence, a value 0 is a minimal one). With no available quality estimator field of the measurements, we only recall that the correlations are less accurate on the boundary of the measured area. We therefore choose to decrease the value of ω, from 1 in almost all the measured area, except on two layers of elements on the boundary of the measured area, driving it linearly to 0 at the boundary within these two layers. As both α and $\boldsymbol{\omega}$ depend on the set of measured dofs, they are different for each measured state.

An equivalent formulation of the updating problem (7) is:

$$\begin{array}{c} \underset{\boldsymbol{u}}{\text{argmin}} \quad g(\boldsymbol{u}, \boldsymbol{v}_\Gamma) \\ \boldsymbol{K}_{\Gamma\Gamma}^\star \boldsymbol{v}_\Gamma = \boldsymbol{f}_\Gamma \end{array} \tag{10}$$

with

$$g(\boldsymbol{u}, \boldsymbol{v}_\Gamma) = \frac{1}{2}(\boldsymbol{A}_\Gamma \boldsymbol{v}_\Gamma - \boldsymbol{u})^T \boldsymbol{K}(\boldsymbol{A}_\Gamma \boldsymbol{v}_\Gamma - \boldsymbol{u}) + \frac{1}{2}\alpha(\boldsymbol{C}\boldsymbol{u} - \boldsymbol{u}_m)^T \boldsymbol{\omega}(\boldsymbol{C}\boldsymbol{u} - \boldsymbol{u}_m) \quad (11)$$

This problem can be interpreted as: control a structure (panel and vertical beams) with dofs on Γ to make the displacement on the measured set close to the measured values $\boldsymbol{u}_m$. As this will be outlined in the following, this problem may be ill-posed, and may require regularization.

Each time an updating is produced, the distance to the measures can be evaluated with:

$$\eta_m = \sqrt{\frac{(\boldsymbol{C}\boldsymbol{u} - \boldsymbol{u}_m)^T \boldsymbol{\omega}(\boldsymbol{C}\boldsymbol{u} - \boldsymbol{u}_m)}{\boldsymbol{u}_m^T \boldsymbol{u}_m}} \quad (12)$$

3.4 Relaxed state $\Omega^{(2)}$

This state, after horizontal beam removal, is similar to the relaxed state in the hole-drilling method used to determine residual stresses. This method has been used for a long time, and more recently, it has been used in conjunction with field measurements in [24, 18, 2] and with finite elements for analyzing the measures, with or without inverse identification, see [29, 26, 23, 13, 5]. Since residual stresses are self-balanced on the considered structure, their energy is null on any displacement change on the same structure. The hole-drilling method therefore relies on a geometric modification. Here, the removal of the horizontal beams may be considered as such a method. Nevertheless, no residual stresses on the configuration $\Omega^{(2)}$ can be reached without a deeper material removal, which is not allowed. So, we can only access to additional residual stresses, or equivalently, we may consider residual stresses on state $\Omega^{(2)}$ as null: $\boldsymbol{\sigma}^{(2)} = 0$.

The measured maximal average curvature of the painted side is about $\rho_m^{(2)} = 0.187\,\mathrm{m}^{-1}$.

The previous model updating approach is used with $\boldsymbol{f}_\Gamma = 0$, and so: $\boldsymbol{v}_\Gamma = 0$ and $\boldsymbol{v} = 0$. In such a case, the displacement $\bar{\boldsymbol{u}}^{(2)}$ mapping $\Omega^{(0)}$ to $\Omega^{(2)}$ is selected as $\boldsymbol{u}$ of the previous approach, for which Equation (10) leads to:

$$\tilde{\boldsymbol{K}}^{(2)} \boldsymbol{u} = \boldsymbol{C}^{(2)} \alpha^{(2)} \boldsymbol{\omega}^{(2)} \bar{\boldsymbol{u}}_m^{(2)} \quad \text{with} \quad \tilde{\boldsymbol{K}}^{(2)} = \boldsymbol{K} + \boldsymbol{C}^{(2)} (\alpha^{(2)} \boldsymbol{\omega}^{(2)}) \boldsymbol{C}^{(2)^T} \quad (13)$$

Since $\bar{\boldsymbol{u}}^{(2)} = \boldsymbol{u}$ is the displacement with respect to $\Omega^{(0)}$, note that the measured displacement with respect to $\Omega^{(0)}$ is used in the right-hand-side. As soon as $\alpha^{(2)}\boldsymbol{\omega}^{(2)}$ is non null, $\tilde{\boldsymbol{K}}^{(2)}$ is obviously symmetric, positive, definite (SPD).

This identification is performed with an error estimation $\eta_m^{(2)} = 16.7\,\%$.

Figure 9 plots the weighting field $\omega^{(2)}$ and the contribution to the error with respect to the measures $[e_m^{(2)}]^2$.

3.5 Initial state $\Omega^{(1)}$

This state, prior to the restoration, corresponds to the (assumed perfect) gluing between the panel and the beams. Model updating from $\Omega^{(0)}$ to $\Omega^{(1)}$ requires the field $\bar{\boldsymbol{u}}^{(1)}$. Alternatively, once $\bar{\boldsymbol{u}}^{(2)}$ has been settled, the more meaningful

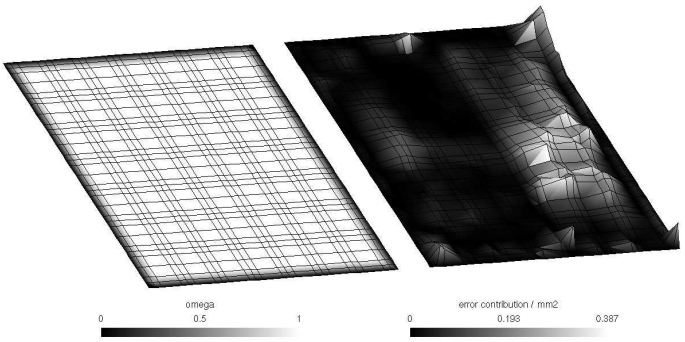

Figure 9: Weighting function $\omega^{(2)}$ (left) and contribution to the error with respect to the measures $[e_m^{(2)}]^2$ (right), after beam removal

displacement field $\boldsymbol{u}^{(1)} = \bar{\boldsymbol{u}}^{(1)} - \bar{\boldsymbol{u}}^{(2)}$ can be searched for. Similarly, $\boldsymbol{u}_m^{(1)} = \bar{\boldsymbol{u}}_m^{(1)} - \bar{\boldsymbol{u}}_m^{(2)}$ on the measured set of state $\Omega^{(1)}$.

The maximal average curvature of the painted side is about $\rho_m^{(1)} = 0.107\,\mathrm{m}^{-1}$, therefore the effect of the horizontal beams is to reduce the free curvature of state $\Omega^{(2)}$.

Since perfect gluing is assumed, the force $\boldsymbol{f}_\Gamma$ is a priori non null, and is not known. In the previous updating approach, we therefore consider $\boldsymbol{v}_\Gamma$ as an unknown. The minimization of the functional g in Equation (10) with respect to both $\boldsymbol{u}$ and $\boldsymbol{v}_\Gamma$, after algebraic manipulations using the property $\boldsymbol{A}_\Gamma^T \boldsymbol{K} = [\boldsymbol{0} \quad \boldsymbol{K}^\star_{\Gamma\Gamma}]$, leads to: $\boldsymbol{v}_\Gamma = \boldsymbol{u}_\Gamma$, and:

$$\tilde{\tilde{\boldsymbol{K}}}^{(1)} \boldsymbol{u} = \boldsymbol{C}^{(1)} \alpha^{(1)} \boldsymbol{\omega}^{(1)} \boldsymbol{u}_m^{(1)} \tag{14}$$

with

$$\tilde{\tilde{\boldsymbol{K}}}^{(1)} = \boldsymbol{K} + \begin{bmatrix} 0 & 0 & 0 \\ 0 & \alpha^{(1)}\boldsymbol{\omega}^{(1)} & 0 \\ 0 & 0 & -\boldsymbol{K}^\star_{\Gamma\Gamma} \end{bmatrix}_{(r,c,\Gamma)}$$

As soon as $\alpha^{(1)}\boldsymbol{\omega}^{(1)}$ is non null, the left-hand-side can be shown to be symmetric, positive but semi-definite only, due to the minus sign before the Schur complement on Γ. Its kernel is the set of control dofs $\boldsymbol{u}_\Gamma$, whose recovering $\boldsymbol{u} = \boldsymbol{A}_\Gamma \boldsymbol{u}_\Gamma$ is null on the measured set, i.e. $\boldsymbol{C}^{(1)} \boldsymbol{A}_\Gamma \boldsymbol{u}_\Gamma = 0$; therefore, if $\boldsymbol{C}^{(1)} \boldsymbol{A}_\Gamma$ is not injective, the problem is ill-posed. An interpretation is the following: if there are too many control dofs on Γ, or too small measured dofs, the control is not unique. The model should therefore be sufficiently refined on the measured region. An alternative solution, used here, is to regularize the functional to be minimized: a regularizing term, avoiding uncontrolled solutions on Γ, but leaving rigid body motions free (these are filtered with measures) can be added to the functional. The simpler choice is:

$$h(\boldsymbol{u}, \boldsymbol{v}_\Gamma) = g(\boldsymbol{u}, \boldsymbol{v}_\Gamma) + \frac{1}{2} \boldsymbol{u}_\Gamma^T \boldsymbol{K}^\star_{\Gamma\Gamma} \boldsymbol{u}_\Gamma \tag{15}$$

which leads to the problem, similar to Equation (13):

$$\tilde{\boldsymbol{K}}^{(1)} \boldsymbol{u} = \boldsymbol{C}^{(1)} \alpha^{(1)} \boldsymbol{\omega}^{(1)} \boldsymbol{u}_m^{(1)} \quad \text{with} \quad \tilde{\boldsymbol{K}}^{(1)} = \boldsymbol{K} + \boldsymbol{C}^{(1)} (\alpha^{(1)} \boldsymbol{\omega}^{(1)}) {\boldsymbol{C}^{(1)}}^T \tag{16}$$

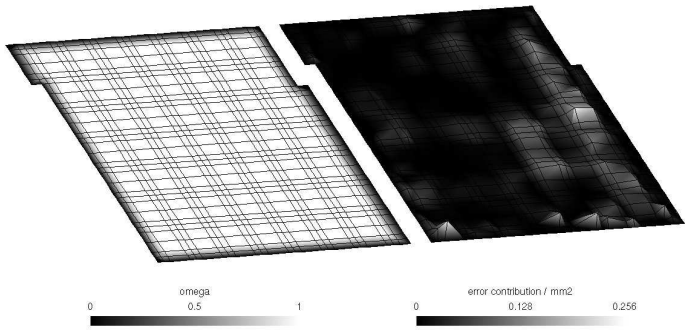

Figure 10: Weighting function $\omega^{(1)}$ (left) and contribution to the error with respect to the measures $[e_m^{(1)}]^2$ (right), for the initial state

and $\boldsymbol{u}^{(1)} = \boldsymbol{A}_\Gamma \boldsymbol{u}_\Gamma$. This identification is performed with an error estimation $\eta_m^{(1)} = 16.6\,\%$.

Figure 10 plots the weighting field $\omega^{(1)}$ and the contribution to the error with respect to the measures $[e_m^{(1)}]^2$.

3.6 Final state $\Omega^{(3)}$

The measured average maximal curvature is $\rho_m^{(3)} = 0.075\,\mathrm{m}^{-1}$. Therefore, though the new beams are less stiff that the older ones, their effect is to render the panel plane. This can be understood by the fact that the relaxed state of the horizontal former beams was itself permanently bent. Therefore, though the stiffness of the structure is lower with the new beams, this restoration act does not automatically reduce short-term residual stresses.

Up to this point, the final state $\Omega^{(3)}$, after replacement of horizontal beams, does not require additional measurements, since the new beams, made with spruce, are supposed to be known with a perfect initial state without residual stress. The beam replacement can therefore be simulated. In a first step, the matching of displacement in the assembly reads: $\underline{\bar{W}}^{(3)} = \underline{\bar{U}}^{(3)}$ at least along the normal vector $\underline{n}$ to Γ (for a frictionless contact model) or for all components (for a perfect gluing), where $\underline{\bar{W}}^{(3)}$ is the displacement field on the new horizontal beams. The panel and vertical beams strain is measured with reference to $\Omega^{(2)}$, and are therefore $\boldsymbol{\varepsilon}(\underline{U}^{(3)}) = \boldsymbol{\varepsilon}(\underline{\bar{U}}^{(3)}) - \boldsymbol{\varepsilon}(\underline{\bar{U}}^{(2)})$. This leads to a classical elastic problem on $\Omega^{(0)}$ with a prestress $\bar{\boldsymbol{\sigma}}^{(2)} = \boldsymbol{D}\boldsymbol{\varepsilon}(\underline{\bar{U}}^{(2)})$ on the panel and vertical beams, and $\boldsymbol{\varepsilon}(\underline{\bar{U}}^{(3)})$ as unknown. This problem is semi-definite positive and the displacement solution is obtained up to an undetermined global rigid body motion (rbm). With this ideal geometry of the new horizontal beams, and a perfect gluing condition, the average simulated curvature is $0.011\,\mathrm{m}^{-1}$ and the error estimation $\eta_m^{(3)} = 62\,\%$ (the unknown rbm of the problem for state $\Omega^{(3)}$ is selected in order to minimize $\eta_m^{(3)}$).

To get a more realistic model, one has to take into account the fact that, in order to allow the mounting of the new beams, their height had to be reduced when compared to the old ones. With an estimated height reduction of 1.25 mm, the simulation of the state $\Omega^{(3)}$ is performed with an elastic 2-body problem with

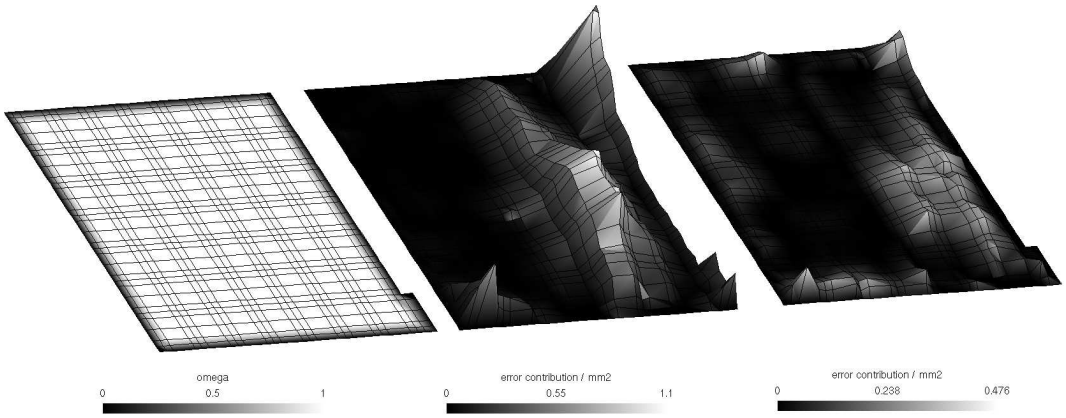

Figure 11: Weighting function $\omega^{(3)}$ (left) and contribution to the error with respect to the measures $[e_m^{(1)}]^2$ with perfect assembly (middle) and a contact with gap (right), with beam replacement

					perfect gluing		contact	
n_e	$\eta_m^{(1)}$	$\sigma_{VM}^{(1)}$	$\eta_m^{(2)}$	$\sigma_{VM}^{(2)}$	$\eta_m^{(3)}$	$\sigma_{VM}^{(3)}$	$\eta_m^{(3)}$	$\sigma_{VM}^{(3)}$
7788	16.6 %	12.3	16.7 %	0	62 %	2.2	26 %	1.1
35094	8.4 %	18.6	14.4 %	0	82.3 %	4.15	28 %	1.7

Table 2: Numerical values obtained with two discretization levels: n_e is the number of finite elements; stress levels are given in MPa

unilateral contact conditions, and the obtained average simulated curvature is $0.064\,\mathrm{m}^{-1}$, with $\eta_m^{(3)} = 26\,\%$.

Figure 11 plots the weighting field $\omega^{(3)}$ and the contributions to the error with respect to the measures $[e_m^{(3)}]^2$, depending on the assembly model.

4 Estimation of the residual stresses

With the previous developments, and still assuming small perturbations in all of the following, the computed residual stresses on the panel are easily obtained:

$$\boldsymbol{\sigma}^{(2)} = 0 \tag{17}$$

$$\boldsymbol{\sigma}^{(1)} = \boldsymbol{D}\boldsymbol{\varepsilon}(\underline{U}^{(1)}) = \boldsymbol{D}\boldsymbol{\varepsilon}(\bar{\underline{U}}^{(1)}) - \bar{\boldsymbol{\sigma}}^{(2)} \tag{18}$$

$$\boldsymbol{\sigma}^{(3)} = \boldsymbol{D}\boldsymbol{\varepsilon}(\underline{U}^{(3)}) = \boldsymbol{D}\boldsymbol{\varepsilon}(\bar{\underline{U}}^{(3)}) - \bar{\boldsymbol{\sigma}}^{(2)} \tag{19}$$

The von Mises component of these residual stresses are depicted in Figure 12. Table 2 recalls the obtained numerical values, for the present discretization with $n_e = 7788$ elements, and with a finer discretization of $n_e = 35094$ elements (two thirds of them are 8-node cubes, the remaining ones are 6-node prisms). The residual stress estimation is still satisfactory, except for the perfect gluing state $\Omega^{(3)}$ whose model is erroneous.

Though it is not a systematic result, the present restoration acts decreases the residual stress in the panel: the maximum von Mises stress σ_{VM} before

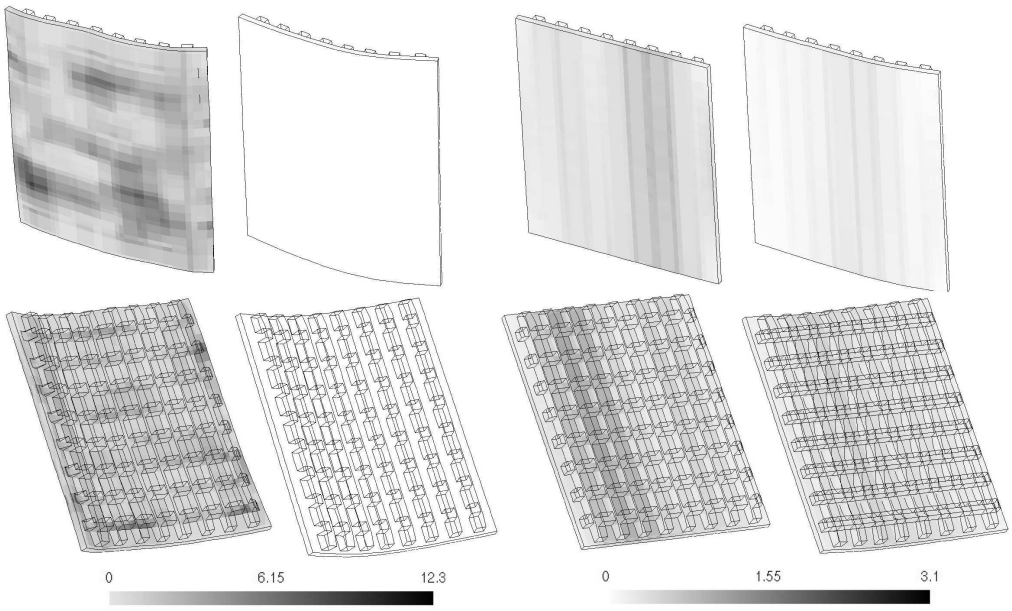

Figure 12: Numerical results (coarse discretization): residual stresses / MPa on the panel (displacement amplified 10 times). From left to right: $\Omega^{(1)}$; $\Omega^{(2)}$; $\Omega^{(3)}$, perfect assembly; $\Omega^{(3)}$, contact with gap

restoration is 18.6 MPa, and is 1.7 MPa after restoration (for the assembly with 1.25 mm gap and the finer discretization).

5 Conclusions and outlooks

In this article, we exemplify that a restoration act on a painted panel of cultural heritage can be considered as a mechanical test, and that with field measurements and modeling, information can be drawn on the structure. Experimental data and numerical modeling are used together to analyze this test, with a model updating approach. This allows to estimate the residual stresses in the structure before and after the restoration.

Though it is the case here, the replacement of old horizontal beams with less stiff new ones does not necessarily decrease the residual stress, since the old beams may exhibit permanent curvature. An other solution would have been a dedicated shape of the replacement parts on an artwork, as in [9, 27]. Indeed such a shape could be designed for the new beams: for instance, taking only into account a curvature $\rho_m^{(3)}$ for sawing them, could decrease again the residual stresses.

The somehow large discrepancies between the model and the measurements for the restored panel may arise from different sources:

- the model does not take into account 2 cracks on the panel;
- the mounting of the new beams can have damaged the panel;

- a too rough estimation of elastic parameters (the identification performed here concerns the shape updating, or the residual stress identification, and not the material characteristics);
- the neglected viscoelastic behavior.

The final replacement of the horizontal beams of the cradle are used as a verification step for the model. An other interesting tool to check the validity of the model would be a local contribution to the error in order to locate the areas where the model is incompatible with the measures. This could be the role of the term $e^2 = \frac{1}{2}(\boldsymbol{u}-\boldsymbol{v})^T \boldsymbol{K}(\boldsymbol{u}-\boldsymbol{v})$ in the cost function to be minimized, if the matching to the measures on the restored artwork is also performed.

Once established, such a model can serve as a predictory tool for assessing risks on the artwork, useful for restorers and conservators, by allowing virtual simulation of the influence of several conservation conditions, and possibly several restoration acts.

Acknowledgements

The authors wish to thank Emmanuel Maurin (LRMH, Laboratoire de Recherche des Momunents Historiques) for fruitful discussion on the restoration technique, Daniel Jaunard and Patrick Mandron (restorers), and Marie-Claude Leonelli (DRAC, Direction Régionale des Affaires Culturelles) for getting access to the panel painting. This work has been supported by European COST Action IE0601 'Wood Science for Conservation of Cultural Heritage'[1].

References

[1] S. Avril, M. Bonnet, A.-S. Bretelle, M. Grédiac, F. Hild, P. Ienny, F. Latourte, D. Lemosse, S. Pagano, E. Pagnacco, and F. Pierron. Overview of identification methods of mechanical parameters based on full-field measurements. *Experimental Mechanics*, 48(4):381–402, 2008.

[2] A. Baldi. Full field methods and residual stress analysis in orthotropic material. I Linear approach. *International Journal of Solids and Structures*, 44(25-26):8229–8243, 2007.

[3] S. Braovac, R. Lochen, B. Aarseth, and A. Sommer-Larsen. The viking ship finds: Preservation challenges and the search for potential solutions. In *First meeting of the COST Action IE0601 Wood Science for Conservation of Cultural Heritage*, Tervuren, 2007.

[4] S. Calloch, D. Dureisseix, and F. Hild. Identification de modèles de comportement de matériaux solides : utilisation d'essais et de calculs. *Technologies et Formations*, 100:36–41, 2002. In french.

[5] J. F. Cárdenas-García and S. Preidikman. Solution of the moiré hole drilling method using a finite-element-method-based approach. *International Journal of Solids and Structures*, 43(22-23):6751–6766, 2006.

[1] http://www.woodculther.org

[6] P. Cavagnero and R. Revelli. Numerical model application for the restoration of the Racconigi Royal Park (CN, Italy). *Journal of Cultural Heritage*, 10(4):514–519, 2009.

[7] P. Chassagne, E. Bou-Saïd, A. Ceccotti, J.-F. Jullien, and M. Togni. The contribution of numerical simulation for the diagnosis of the conservation of art objects: Application to Antonio Santucci's armillary sphere of the 16th century. *Journal of Cultural Heritage*, 8(3):215–222, 2007.

[8] P. Chassagne, P. Dionisi Vici, E. Vidal-Sallé, L. Uzielli, and J.-F. Jullien. Mechanical consequences of hygroscopic variations on wooden panel paintings: development of a predictive model. In *Proceedings of the 4th International Conference of joint meeting of European Society for Wood Mechanics and COST Action E35*, Florence, Italy, 2006.

[9] M. Ciatti, C. Castelli, and A. Santacesaria. *Dipinti su tavola, la tecnica e la conservazione dei supporti*. Edifir, 1999. In italian.

[10] D. Dureisseix, J. Gril, and O. Arnould. Mechanical modeling of the activity of the flexible frame. In J.-P. Mohen, M. Menu, and B. Mottin, editors, *Mona Lisa, inside the painting*, chapter II.6. Abrams, New York, 2006.

[11] D. Guitard. *Mécanique du matériau bois et composites*. Cepadues Editions, 1987. In french.

[12] P. Ladevèze, D. Nedjar, and M. Reynier. Updating of finite element models using vibration tests. *AIAA Journal*, 32(7):1485–1491, 1994.

[13] F. Lanza di Scalea, S. S. Hong, and G. L. Cloud. Whole-field strain measurement in a pin-loaded plate by electronic speckle pattern interferometry and the finite element method. *Experimental Mechanics*, 38(1):55–60, 1998.

[14] S. Leconte, M. Vion, and C. Clarke. Attempt to find the ancient sound: from the modelisation to the reconstruction of the Erard Piano in Musée de la musique. In *International Conference on Wooden Cultural Heritage: Evaluation of Deterioration and Management of Change*, Hamburg, 2009. COST Action IE0601 Wood Science for Conservation of Cultural Heritage.

[15] H. Maigre and F. Morestin. Image correlation applied to wood painting. In *Photomechanics 2008*, Loughborough, UK., 2008.

[16] B. Marcon. *Hygromécanique des panneaux en bois et conservation du patrimoine culturel*. PhD thesis, University Montpellier 2, Università degli studi di Firenze, 2009. In french.

[17] E. Mele, A. De Luca, and A. Giordano. Modelling and analysis of a basilica under earthquake loading. *Journal of Cultural Heritage*, 4(4):355–367, 2003.

[18] D. V. Nelson, A. Makino, and T. Schmidt. Residual stress determination using hole drilling and 3D image correlation. *Experimental Mechanics*, 46(1):31–38, 2006.

[19] M. Nesme, Y. Payan, and F. Faure. Efficient, physically plausible finite elements. In J. Dingliana and F. Ganovelli, editors, *Proceedings of EUROGRAPHICS 2005*, 2005.

[20] A. Rafiee, M. Vinches, and C. Bohatier. Modelling and analysis of the Nîmes arena and the Arles aqueduct subjected to a seismic loading, using the Non-Smooth Contact Dynamics method. *Engineering Structures*, 30(12):3457–3467, 2008.

[21] A. Rothe. Critical history of panel painting restoration in italy. In K. Dardes and A. Rothe, editors, *The Structural Conservation of Panel Paintings: Proceedings of a Symposium at the J. Paul Getty Museum*, pages 188–199, Los Angeles, 1998. The Getty Conservation Institute.

[22] S. Saft and M. Kaliske. Supporting the restoration of historical pianofortes by numerical simulation. In *International Conference on Wooden Cultural Heritage: Evaluation of Deterioration and Management of Change*, Hamburg, 2009. COST Action IE0601 Wood Science for Conservation of Cultural Heritage. 8 pages.

[23] G. S. Schajer. Advances in hole-drilling residual stress measurements. *Experimental Mechanics*, 50(2):159–168, 2009.

[24] G. S. Schajer and M. Steinzig. Full-field calculation of hole drilling residual stresses from electronic speckle pattern interferometry data. *Experimental Mechanics*, 45(6):526–532, 2005.

[25] R. Schmedding and M. Teschner. Inversion handling for stable deformable modelling . *The Visual Computer: International Journal of Computer Graphics*, 24(7):625–633, 2008.

[26] D. Shaw and H. Y. Chen. A finite-element technique to analyze the data measured by the hole-drilling method. *Experimental Mechanics*, 30(2):120–123, 1990.

[27] L. Uzielli and O. Casazza. *Conservazione dei dipinti su tavola*. Nardini Editore, 1992. In italian.

[28] M. R. Valluzzi, A. Bondì, F. da Porto, P. Franchetti, and C. Modena. Structural investigations and analyses for the conservation of the 'Arsenale' of Venice. *Journal of Cultural Heritage*, 3(1):65–71, 2002.

[29] F. Zhang, A. J. Kassab, and D. W. Nicholson. A boundary element solution of an inverse elasticity problem and applications to determining residual stress and contact stress. *International Journal of Solids and Structures*, 34(16):2073–2086, 1997.